



# Synthesis, physical study and efficient photocatalytic activity of FeTe<sub>2</sub>

A. Mami<sup>1</sup> · K. Ben Messaoud<sup>2</sup> · O. Kamoun<sup>2</sup> · M. Amlouk<sup>2</sup>

Received: 24 October 2018 / Accepted: 7 February 2019 / Published online: 14 February 2019  
© Springer Science+Business Media, LLC, part of Springer Nature 2019

## Abstract

This paper covers a successfully grown process of iron ditelluride (FeTe<sub>2</sub>) thin films deposited on glass substrates. Structural, morphological and optical properties were investigated by means of X-ray diffraction (XRD), scanning electron microscopy (SEM) and optical measurements. As well as, photoluminescence (PL) spectroscopy, electrical, thermal and photocatalytic performance of iron ditelluride thin films were determined using photoluminescence spectroscopy, impedance spectroscopy technique and electro-pyroelectric method, for the first time in literature. The XRD results revealed that preferentially orientation along (111) direction at 2θ value of approximately 32.03° have been observed for FeTe<sub>2</sub> films. Besides, the impedance spectroscopy was used to determine the resistance R, the electrical capacitance C<sub>e</sub>, as well as the angular frequency of the maximum peak ω<sub>m</sub> depending on the effect of temperature. In addition, the activation energy was found equal to E<sub>g</sub> = 0.23 eV for iron ditelluride thin film. The thermal measurement for the composite revealed the thermal conductivity and thermal diffusivity of FeTe<sub>2</sub> are about 1.2 W m<sup>-1</sup> K<sup>-1</sup> and 3.9 × 10<sup>-7</sup> m<sup>2</sup> s<sup>-1</sup>, respectively. The photocatalytic activity and stability of this material under visible light irradiation towards the degradation of methylene blue dye was carried out. The iron ditelluride composite exhibited a high photocatalytic degradation performance.

## 1 Introduction

Since the discovery of the superconductivity phenomenon by 2008 on La (O<sub>1-x</sub>F<sub>x</sub>) FeAs materials [1], a large number of iron-based superconductors have been discovered due to many efforts to determine their high temperature superconductors (HTSC). Indeed, this discovery seems providing a new playground in the HTSC group with the current record-holding T<sub>c</sub> of 56 K which are actually the quintuples Gd<sub>1-x</sub>Th<sub>x</sub>FeAsO and Sr<sub>1-x</sub>Sm<sub>x</sub>FeAsF [2, 3]. Among iron-based superconductors family such as FeTe<sub>0.8</sub>S<sub>0.2</sub> and FeTe<sub>0.7</sub>S<sub>0.3</sub> polycrystalline samples were found. These compounds were obtained using solid state reaction with a three-step procedure and exhibited a zero resistivity because of the reduction of Fe excess which is related to the formation of FeTe<sub>2</sub> and Fe<sub>3</sub>O<sub>4</sub> impurity phases. The latest phenomenon

was observed not only in oxygen post-annealed samples but also in as-grown ones [4].

In addition, FeX<sub>2</sub> (X = S, Se, Te) chalcogenides have attracted attention in many fields thanks to their relative simple synthesis protocols, simple crystal structures and they exhibit semiconducting behaviour [5–7]. Besides, under certain ambient conditions, the previous chalcogenides exhibit marcasite structure while in high boundary values of temperature and pressure synthesis leads rather to more stable pyrite structure [8].

FeTe<sub>2</sub> is an archetypal material that has been prepared by several synthetic methods [9, 10]. Song and Bochmann [11] synthesized tellurium complex of the type [M<sub>2</sub>{Bu<sub>2</sub><sup>t</sup>P(E)NR}<sub>2</sub>] as precursors for the gas-phase deposition of FeTe<sub>2</sub> film. Also, preparation route using a simple spray pyrolysis technique and optical properties of the iron telluride thin films has been explored by Ben Messaoudi et al. [12, 13]. However, photoluminescence, thermal, electrical characterisations and photocatalytic performance of these films have not been studied. Herein, we report structural, optical, photoluminescence, thermal, electrical properties and photocatalytic behaviour of FeTe<sub>2</sub> thin films with marcasite structure. These samples were synthesised by a simple protocol consisting on anneal amorphous iron oxide layers. Afterwards, they have been explored by XRD, SEM, optical

✉ A. Mami  
amelmami@gmail.com

<sup>1</sup> U.R. Photopyroelectric, IPEIN, Merazka, BP 62,  
8000 Nabeul, Tunisia

<sup>2</sup> Unité de Physique des Dispositifs à Semi-conducteurs  
(UPDS), Faculté des Sciences de Tunis, Tunis El Manar  
University, 2090 Tunis, Tunisia

measurements, PL spectroscopy, impedance analyser and electro-pyroelectric technique. The electrical and impedance measurements, as well thermal properties of iron ditelluride thin films were determined, for the first time in literature. Thanks to this work, we have confirmed that such compound may has interesting photocatalytic performance.

## 2 Experimental techniques

### 2.1 Sample preparation

FeTe<sub>2</sub> thin films were deposited on glass substrates and placed on a hot plate heated at 350 °C [12, 13]. Those films have been prepared using an aqueous solution of FeCl<sub>3</sub>·6H<sub>2</sub>O (0.015 M). Then, 50 ml of the solution was sprayed with nitrogen as a gas carrier by means of a nozzle allowing a jet flow rate of 4 ml/min. The obtained amorphous iron oxide films were placed with 20 mg of tellurium in a vacuum (~10<sup>4</sup> Pa) sealed Pyrex tube. The latter procedure has been employed a heat treatment under tellurium atmosphere in an electric tubular oven at temperature 530 °C for 24 h. The thickness of these films was of the order of 400 nm using the interference fringes method [14].

### 2.2 Characterization techniques

X-ray diffraction analysis of all prepared thin films was performed by a copper source diffractometer (Analytical X Pert PROMPD), with the wavelength ( $\lambda = 1.54056 \text{ \AA}$ ). Diffractograms were obtained by varying angle ( $2\theta$ ) from 3° to 70°. Besides, the surface morphologies of the FeTe<sub>2</sub> thin films were performed by scanning electron microscopy (JSM-5400). Further, the optical measurements, in the UV–Vis range were carried out using a Shimadzu UV 3100 double-beam spectrophotometer, within a (250–2500 nm) wavelength range. The PL measurements were performed at room temperature in the range of 470–900 nm using a HORIBA Jobin yvon spectrometer. This kind of study requires an excitation by He–Cd laser ( $\lambda = 325 \text{ nm}$ , 50 Hz).

In addition, the electrical study of the prepared FeTe<sub>2</sub> thin films were determined to study the impedance spectroscopy by means of a Hewlett-Packard 4192 analyzer that is equipped to a computer for data acquisition. The study has been made in the temperature range (450–480 °C) with frequency of (5–13,000 kHz) and forced us to implement two electrodes on their extremities using a conductive silver paste [15, 16].

Moreover, in electro-pyroelectric (EPE) experiments on the back-scattering geometry, a sinusoidally modulated voltage was flowed through the serpentine at a metal contact. As a result, an oscillatory heat flux was diffused through the silpad 900S thanks to Joule heating effects. The latter is a thermally

conductive insulation material which is composed of silicon and fiberglass compounds in order to avoid a short circuit. Indeed, Silpad 900S was deposited on a polyvinylidene fluoride (PVDF) film of 28  $\mu\text{m}$  thickness, which produced a rise of temperature over the time at its interface. As a result, a pyroelectric current was generated. The EPE amplitude and phase signals were acquired by use a preamplifier, a Stanford SR 530 lock-in amplifier and a computer-based data acquisition via a RS 232 interface.

Finally, the photocatalytic performance of prepared FeTe<sub>2</sub> films was evaluated via evaluating the discoloration of an aqueous solution of methylene blue (MB) under irradiation with visible and solar light. For the photodegradation of MB dye, we used a 50 ml beaker with 10 mg of prepared photocatalysts.

Before the irradiation, the obtained solution was placed in a dark for 1 h in order to obtain the adsorption–desorption equilibrium. The initial concentration  $C_0$  and the pH value of the MB solution were taken respectively as  $C_0 = 10^{-5} \text{ M}$  and pH 7.2. Afterward, 10 ml of the solution was taken out from the prepared mixture using a syringe and the sunlight irradiations of the MB solution were examined every 20 min by a UV–Vis spectrometer to evaluate the decrease in the dye concentration. So, the photocatalytic activities of FeTe<sub>2</sub> samples could be calculated. Indeed, the degradation efficiency of such thin film was described for MB dyes by means of

$$\% = [(C_0 - C)/C_0] \times 100\%. \quad (1)$$

with  $C$  is the concentration of dye solution after irradiation, and  $C_0$  is the preliminary concentration of dye solution.

## 3 Results and discussion

### 3.1 Structural properties

#### 3.1.1 X-ray diffraction

Figure 1 shows X-ray diffraction analysis which proves that this film has a good crystalline state with the appearance of multi peaks of the FeTe<sub>2</sub> orthorhombic phase. In such film we note the formation of FeTe<sub>2</sub> binary material with the crystallites are preferentially orientated along [111] direction at  $2\theta$  value of 32.03°, close to JCPDS file, no.: 00-014-0419 card, as already recorded by Ben Messaoud et al. [12]. The lattice parameters are:  $a = 5.26 \text{ \AA}$ ,  $b = 6.26 \text{ \AA}$ , and  $c = 3.88 \text{ \AA}$ ; these results are in agreement with those of previous studies [17].

To obtain useful information on improving the thin film structure of FeTe<sub>2</sub>, some calculations have been done. The interplanar spacing  $d_{hkl}$  were estimated by using the Bragg equation:

$$2d_{hkl}\sin\theta = n\lambda \quad (2)$$

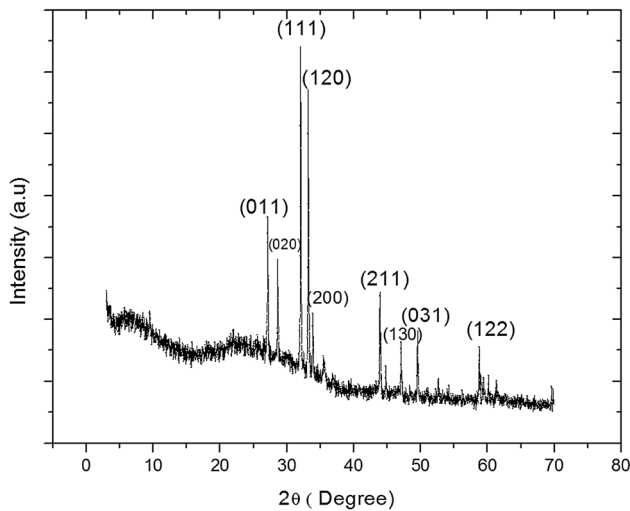


**Fig. 1** XRD pattern of nanocrystalline FeTe<sub>2</sub> annealed at 530 °C

where  $\lambda$  is the X-ray wavelength,  $\theta$  is the Bragg diffraction angle, and  $n$  is the order of the diffraction (usually  $n = 1$ ).

For the orthorhombic close-packed structure:

$$\frac{1}{d_{hkl}^2} = \frac{h^2}{a^2} + \frac{k^2}{b^2} + \frac{l^2}{c^2} \quad (3)$$

Moreover, some structural parameters such as the crystallite size ( $D$ ), number of crystallites ( $N_c$ ), micro-strain ( $\epsilon$ ), and amount of defects in a crystal defined as the length of dislocation lines per unit volume ( $\delta$ ) could be estimated by the following expressions [18–21]:

$$D = \frac{k_0 \times \lambda}{\beta_{\frac{1}{2}} \cos(\theta)} \quad (4)$$

$$N_c = \frac{\ell'}{D^3} \quad (5)$$

$$\epsilon = \frac{\beta_{\frac{1}{2}}}{4 \tan(\theta)} \quad (6)$$

$$\delta = \frac{1}{D^2} \quad (7)$$

where  $k_0 = 0.90$ ,  $\beta_{\frac{1}{2}} = \sqrt{(\beta_e^2 - \beta_0^2)}$  and  $\ell'$  are the Scherer constant, the full width at half maximum and the thickness of the FeTe<sub>2</sub> layers. With,  $\beta_e$  is measured from the film and  $\beta_0$  is the full width at half maximum related to the XRD peaks.

Calculated values of the grain size, the micro-strain, and the dislocation density of the thin films are summarized in Table 1.

### 3.1.2 SEM observation

The marcasite FeTe<sub>2</sub> was analyzed through scanning electron microscopy, Fig. 2. The result showed that the voids and the shape of ditelluride iron are characterized by irregular and micron-sized polyhedrons. Large particles usually cause a decrease in catalytic active sites; large particles may also affect the catalytic activity of FeTe<sub>2</sub> [17].

### 3.2 Optical study

Figure 3 reveals the optical absorbance  $A$  of the investigated films in the range of 300–1185 nm wavelength at room temperature. It can be seen an absorption band at 300 nm in UV region as well as a broad band spanning between 400 and 800 nm in visible region.

Besides, we can reach the absorption coefficient  $\alpha$  of the material using the following well known formula [22]:

$$\alpha = 2.303 \frac{A}{\ell} \quad (8)$$

with  $A$  the absorbance of the film and  $\ell$  its thickness.

The absorption coefficient  $\alpha$  can be related to the energy gap  $E_g$  of FeTe<sub>2</sub> sprayed thin films from the following Tauc relationship [23–25]:

**Table 1** Structural constants of FeTe<sub>2</sub> thin films

	D (nm)	$N_c$ ( $10^{18} \text{ m}^{-2}$ )	$\epsilon$ ( $10^{-3}$ )	$\delta$ ( $10^{15} \text{ line/m}^2$ )
FeTe <sub>2</sub>	12.0	16.6	1.10	6.90

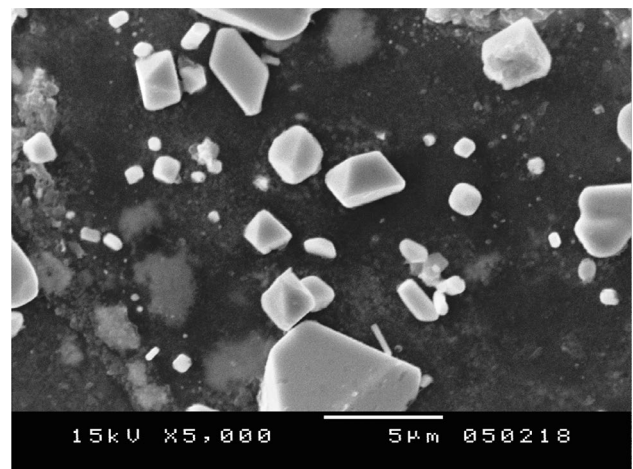


**Fig. 2** SEM microphotograph of surface of as-prepared FeTe<sub>2</sub>

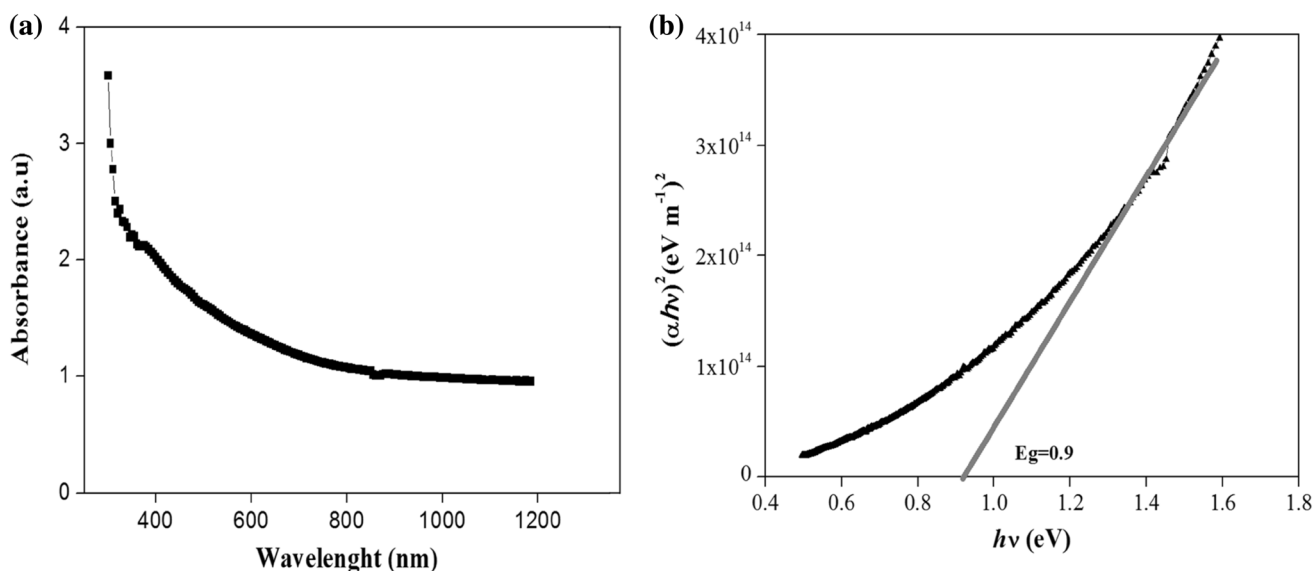


**Fig. 3** **a** Absorbance versus wavelength of FeTe<sub>2</sub> thin film. **b** Tauc-plot of FeTe<sub>2</sub> thin film

$$(\alpha h\nu) = A'(h\nu - E_g)^n \quad (9)$$

where  $A'$  is a constant related to the probability of transition,  $h\nu$  (eV) is the incident photon energy,  $E_g$  (eV) is the energy gap and  $n$  is equal to  $\frac{1}{2}$  for direct band transition.

The optical band gap is evaluated by plotting  $(\alpha h\nu)^2$  versus  $h\nu$  and extrapolating the linear part of the curve, Fig. 3b. So, the intercept (extrapolation) of this plot (straight line) on the energy axis gives the energy band gap value. We notice that the graph has linear part, which indicate direct band gap type behaviour for FeTe<sub>2</sub>.

The calculated values of  $E_g$  of FeTe<sub>2</sub> thin film is of the order of 0.9 eV which fall within the range reported elsewhere [26–28]. These band gap energies for the marcasite Te iron chalcogenide do not suggest a role as a light-absorbing layer in highly efficient solar cells which confirms the previous results.

In fact, this optical study confirms the records of Si et al. [29] and Nie et al. [30], who stated that for deposition temperatures beyond 500 °C, the orthorhombic phase of the oxide Fe<sub>2</sub>O<sub>3</sub> appears and prevents the substitution of oxygen by tellurium.

As result of the incorporation of impurities and excess metal into the iron ditelluride thin film affects the band gap structure and optical transitions which reveals a tail for the density of states of the band gap. The Urbach tail can be obtained using the following empirical Urbach equation [31, 32]:

$$\alpha = \alpha_0 \exp\left(\frac{h\nu}{E_U}\right) \quad (10)$$

where  $\alpha_0$  is a constant and  $E_U$  is the Urbach energy which is given by the slope of the exponential limit. Knowing the

optical gap value, the optical absorption by defects appears at a lower energy. The obtained urbach energy value is about  $E_U = 416$  meV and it appears as a relatively high value because of the structural defects inside the film detailed above.

### 3.3 Photoluminescence (PL)

Room temperature PL spectra were recorded to find the exact band edge emission of the synthesized FeTe<sub>2</sub>.

Figure 4 shows the PL spectrum of FeTe<sub>2</sub> thin film. The iron ditelluride spectrum shows a broad emission band. Actually, in order to understand the origin of the PL peaks, it is required to achieve the de-convoluted following Gaussian profile fitting.

We can notice, from the spectra's Gaussian fitting, six bands in visible and IR regions. In fact, the emissions between 522 and 537 nm could be originated from the recombination of the photogenerated holes with singly ionized charge state of specific defect.

The PL bands of iron ditelluride thin film have indeed a weak emission band located at 578 nm, which may be attributed to the presence of a minority phase of Fe<sub>2</sub>O<sub>3</sub> [33].

### 3.4 Electrical study

Figure 5 represents the Nyquist plot for FeTe<sub>2</sub> sprayed thin film which reflected the variation of the imaginary part ( $Z''$ ) corresponding with the real part ( $Z'$ ) at temperatures ranged between 450 and 480 °C in order to determine the conducting state of FeTe<sub>2</sub> thin film.

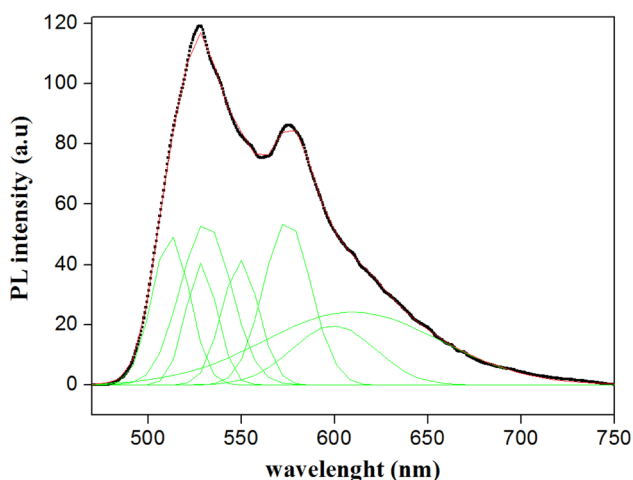


**Fig. 4** Photoluminescence spectra of FeTe<sub>2</sub> thin film

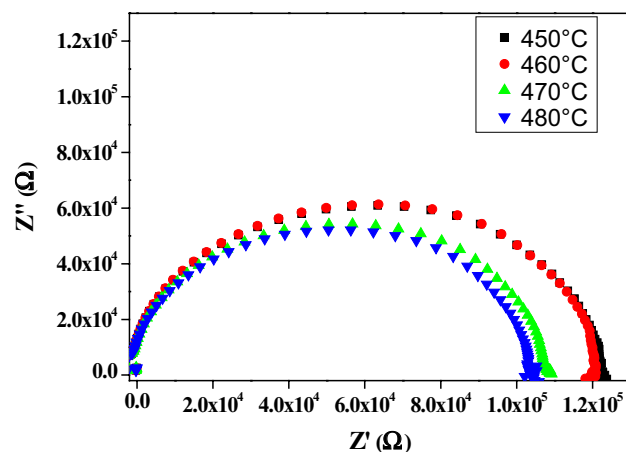


**Fig. 5** Complex impedance diagrams ( $Z''$  vs.  $Z'$ ) at different temperatures

The nyquist diagram shows the presence of only one semi-circle over the entire frequency range which demonstrate that the electrical conduction process arises due to the relaxation model. So, it is noted that each semi-circle may be modeled in terms of an electrical equivalent circuit composed of a resistance  $R$  and a capacitance  $C_e$  associated in parallel that is attributable to the grains in the conduction mechanism.

In addition, the variation of the real impedance  $Z'$  decreases when the temperature increase. Therefore, we can estimate that the electrical conductivity is thermally activated; and so we assume a semiconductor behavior of such material.

Figure 6 shows the variation of  $Z''$  against angular frequency ( $\text{Ln}(\omega_m)$ ) at different temperatures of FeTe<sub>2</sub> thin film. It is noted that the imaginary part of the complex impedance ( $Z''$ ) spectra has a relaxation peak which shifts

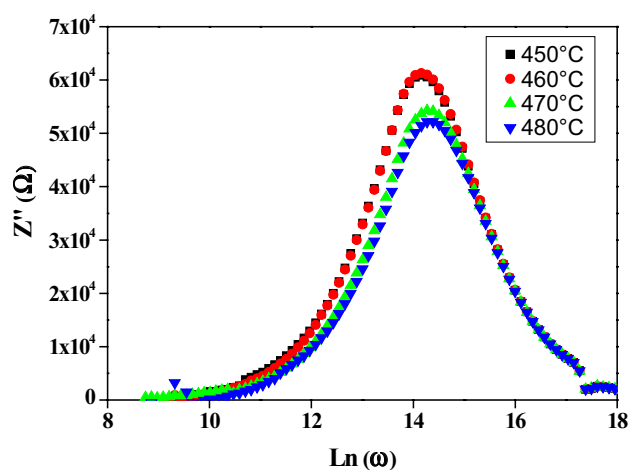


**Fig. 6** Angular frequency dependence ( $\text{Ln}(\omega_m)$ ) of the imaginary part of the complex impedance ( $Z''$ ) at different temperatures

**Table 2** Values of electrical parameters at different temperatures of FeTe<sub>2</sub> thin film

Measurement temperature (°C)	$\text{Ln}(\omega_m)$	$\omega_m$ ( $10^6$ )	$R$ ( $10^5 \Omega$ )	$C_e$ ( $10^{-12}$ F)
450	14.2	1.60	1.22	5.12
460	14.2	1.60	1.19	5.25
470	14.4	1.83	1.06	5.15
480	14.4	1.83	1.02	5.35

slightly to the higher values of frequency as the temperature is increased.

We first investigated the angular frequency of the maximum peak  $\omega_m$  that is expressed by the following equation:

$$\omega_m = \frac{1}{\tau} = \frac{1}{RC_e} \quad (11)$$

with  $\tau$  is the relaxation time.

As listed in Table 2, it is found that the calculated  $C_e$  value is of the order of 5 pF in the temperature range 450–480 °C. Also, we notice that the  $R$  value decreases with the rise of the temperature, as well as the expected value of the  $\omega_m$  has been increased with the temperature.

As shown in Fig. 7, the frequency evolution of the total conductivity at different temperatures is independent at low frequencies, which may be attributed to dC contribution. In contrast, for the high frequencies, the variation of the total conductivity increases linearly with the frequency characterizing the measured AC conductivity ( $\sigma_{AC}$ ).

Following Jonscher's universal power law, the frequency dependence of AC conductivity is introduced by the following equation [34, 35]:

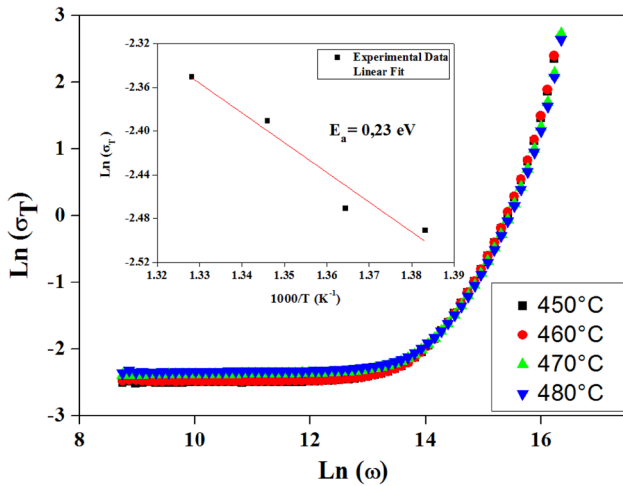


**Fig. 7** Frequency dependence of  $\ln(\sigma_T)$  versus  $\ln(\omega)$  at different temperatures

$$\sigma_{AC} = \sigma_T - \sigma_{dC} = A''\omega^S, \tag{12}$$

with  $w$  is the angular frequency, the exponent  $S$  can be in  $0 \leq S \leq 1$  domain,  $A''$  is a complex proportionality constant and  $\sigma_{dC}$  is the dC conductivity.

The AC conductivity is frequency dependent and it shifts to a higher frequency with an increase of the temperature, which is consistent with the observed shift of the relaxation frequency.

In fact, as seen in Fig. 7, an enlargement of the electrical conductivity dependant temperature in the studied material is noticed which was previously confirmed by the decrease of resistance values  $R$  with temperature increasing (see Table 2).

As displayed in the insets of Fig. 7, the expression of  $\ln(\sigma_T)$  as a function of  $(1000/T)$  has a linear behavior and follows the Arrhenius model [36, 37]:

$$\sigma_T = \sigma_0 \exp\left(\frac{-E_a}{k_B T}\right) \tag{13}$$

with  $k_B$  is the Boltzmann constant,  $\sigma_0$  is a constant and  $E_a$  is the activation energy.

The activation energy  $E_a$  value is about  $E_a = 0.23$  eV which let us mention that the carrier transport mechanism is a thermally activated process.

### 3.5 Thermal investigation

In this paper, an electro-pyroelectric (EPE) technique on the front detection configuration has been used to reach both the thermal conductivity  $k$  and thermal diffusivity  $D$  [38–40]. Indeed, Fig. 8 displays the configuration that is made of five adjacent layers: air (a), insulator sample (2), PVDF film (p), investigated sample (1), substrate (S) and backing (b). In

fact, it is practical to normalize the EPE signals of the samples to the one obtained without the studied sample ( $\ell_1 = 0$ ).

The theoretical model of the EPE normalized voltage signal is a complex function of frequency modulation and thermal properties of the studied sample [38]. From a comparison between the experimental and theoretical curves of the normalized EPE signals using mathematical software (Maple.13), thermal conductivity and diffusivity values of  $\text{FeTe}_2$  thin film were determined. Finally, thermal effusivity  $e$  and volume heat capacity  $C_{th}$  can be obtained from the following equations:

$$C_{th} = \frac{e}{\sqrt{D}}, \tag{14}$$

$$k = e \times \sqrt{D} \tag{15}$$

Figure 9 shows the best fits found between experimental and theoretical amplitudes and phases of the normalized EPE signal as a function of modulation frequency for sprayed  $\text{FeTe}_2$  thin film. The best coincidences between these curves are obtained for given values of both thermal

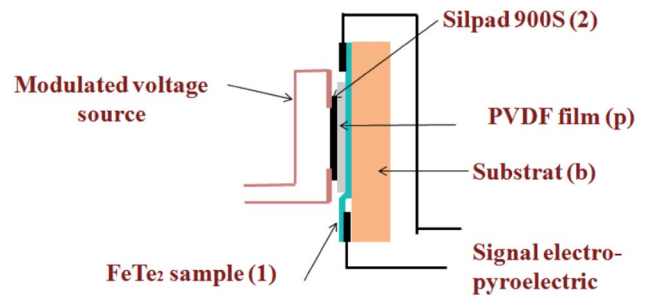


**Fig. 8** Geometry of electro-pyroelectric cell in front detection configuration

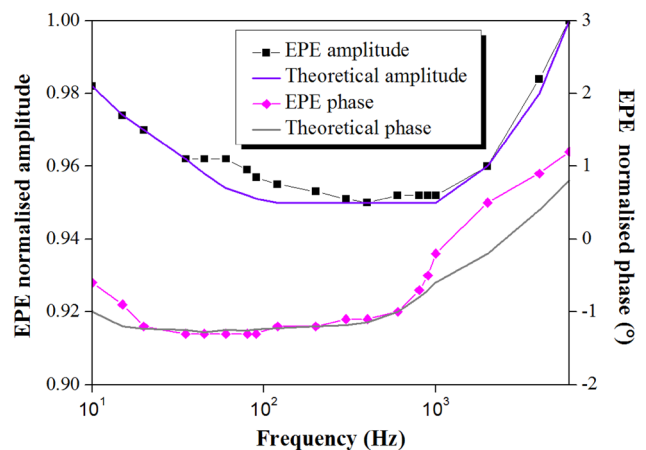


**Fig. 9** Experimental (dots) and theoretical (line) normalized amplitude and phase of the electro-pyroelectric signal for  $\text{FeTe}_2$  according to the frequency modulation

conductivity and diffusivity of the studied sample. Then, we rely on Eqs. (14) and (15) to extract the thermal effusivity and the heat capacity of the studied film. The obtained values are listed in Table 3.

The surprising low thermal conductivity of  $\text{FeTe}_2$ , as shown in Table 3, makes it as a possible candidate (lower than  $2 \text{ W m}^{-1} \text{ K}^{-1}$ ) for practical thermoelectric applications. The phonon mean free path is very sensitive to the grain boundary and disorder effect that could enhance the scattering process and suppress the phonon mean free path [41]. The excess of Te element can be results to the low value of the thermal conductivity as seen by the bright zones on the surface of  $\text{FeTe}_2$  film observed in Fig. 2.

Unfortunately, as there is no report on the thermal properties of bulk  $\text{FeTe}_2$ , therefore, comparison with experimental data from other sources is impractical.

In the past decade years, a few studies have been motivated to explore thermal properties of other chalcogenides family such as  $\text{FeSb}_2$ . The thermal conductivity of the latter nanocomposite sample is about  $2 \text{ W m}^{-1} \text{ K}^{-1}$  which is well comparable or even higher than that of iron ditelluride sample ( $1.2 \text{ W m}^{-1} \text{ K}^{-1}$ ) [42].

### 3.6 Photocatalytic activity

In Fig. 10, it is found that the absorbance of methylene blue (MB) in the presence of  $\text{FeTe}_2$  thin film under solar light decreases continuously with the variation of illumination time from 0 to 100 min. In the presence of sample  $\text{FeTe}_2$ , MB solution becomes totally colorless after 100 min of irradiation, signifying the total breaking down of dye molecules by  $\text{FeTe}_2$  nanoparticles. Thus, we conclude that the functional group responsible for the characteristic color of MB dyes is decomposed and consequently we have observed a quick vanishing of the absorption bands of MB dyes.

The degradation efficiency of the studied thin film for MB dyes was given in Fig. 11a. The formula used to calculate the rate of the degradation efficiency is given by the Eq. (1) [43, 44].

The photocatalytic reaction in chosen time  $t$  can be estimated according to Eq. (16):

$$\ln C_0/C = k_r t \quad (16)$$

The constant  $k_r$  is defined as rate constant for degradation.

As shown in Fig. 11b, the plot of  $\ln (C_0/C)$  as a function of irradiation time gives a straight line, which proves the

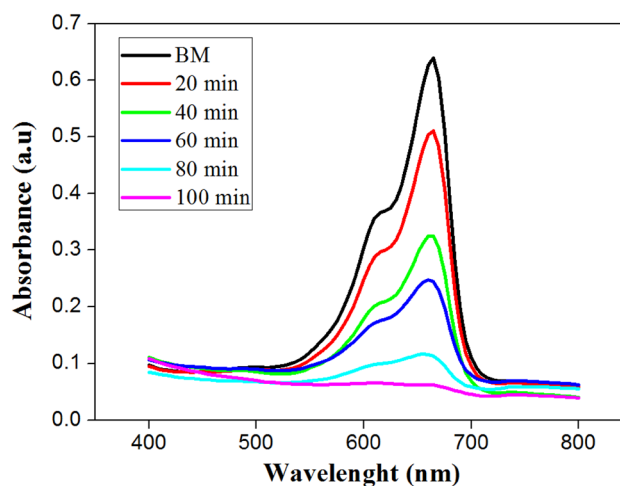


Fig. 10 The photodegradation curves of MB in the presence of  $\text{FeTe}_2$  thin film under solar light

first-order kinetic of the photocatalytic decomposition reaction [45, 46].

So,  $k_r$  can be obtained from the slope of the curves in Fig. 11b and the evaluated value is  $2.33 \times 10^{-2} \text{ min}^{-1}$ .

Venkata Reddy et al. [47] reported that  $\text{CdO}/\text{ZnO}$  hybrid photocatalyst exhibited better photocatalytic activity and photostability, compared to  $\text{ZnO}$  and  $\text{CdO}$  ones, thanks to its high degradation rate constant ( $2.25 \times 10^{-2} \text{ min}^{-1}$ ).

Indeed, the above result shows that  $\text{FeTe}_2$  obtained by this simple route had greater degradation rate constant compared to the  $\text{CdO}/\text{ZnO}$  hybrid sample which its combination of unlike semiconductor oxides can decrease the electron–hole pair separation under light irradiation leading to a relatively high photocatalytic performance [47].

However,  $\text{FeTe}_2$  material synthesized by this protocol seems more interesting than the other materials since it provides the best photocatalytic behaviour.

The suitable band gap in the thin materials can support transfer of electrons and holes to the surface under light, these electrons and holes can increase the photoreaction.

## 4 Conclusion

In this work, ditelluride thin film has been successfully prepared by a simply protocol. XRD studies reveal the orthorhombic phase of  $\text{FeTe}_2$  with the crystallites is preferentially orientated along [111] direction at  $2\theta$  values of  $32.03^\circ$ . Moreover, the obtained value of energy gap of the sprayed thin film  $\text{FeTe}_2$

Table 3 Thermal parameters of sprayed  $\text{FeTe}_2$

	$k$ ( $\text{W m}^{-1} \text{ K}^{-1}$ )	$D$ ( $10^{-7} \text{ m}^2 \text{ s}^{-1}$ )	$C_{th}$ ( $\text{J K}^{-1} \text{ m}^{-3}$ )	$e$ ( $10^2 \text{ J K}^{-1} \text{ m}^{-2} \text{ s}^{-1/2}$ )
$\text{FeTe}_2$	$1.20 \pm 0.02$	$3.90 \pm 0.02$	307	19.2

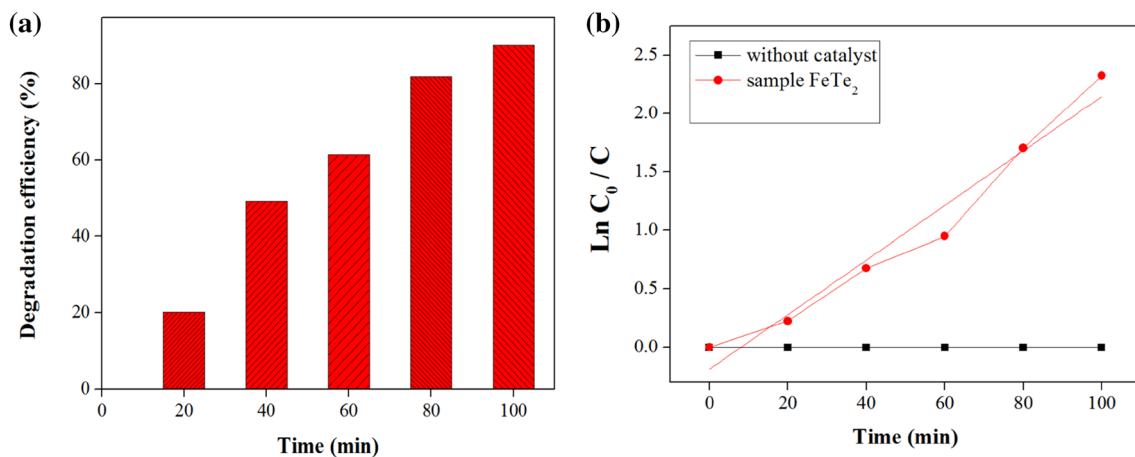


**Fig. 11** Comparison of **a** degradation rate and **b** degradation kinetics of MB dye under different conditions

is  $E_g = 0.9$  eV do not suggest a role as a light-absorbing layer in highly photovoltaic solar conversion. On the other hand, the Nyquist plot, the electrical parameters, as well as the thermal properties for FeTe<sub>2</sub> thin have been carried out. The photocatalytic activity of the synthesized FeTe<sub>2</sub> thin film was evaluated for degradation of MB dye which demonstrated 90% degradation after 100 min of visible illumination.

Despite many research efforts, no attempts have been made to determine their magnetic and dielectric behaviors, as well as their thermoelectric figures of merit. It would be valuable for future research to understand properties and behavior of FeTe<sub>2</sub> compounds which we suggest to use it for possible thermoelectric applications and for sensitivity ones.

## References

1. Y. Kamihara, T. Watanabe, M. Hirano, H. Hosono, Iron-based layered superconductor La[O<sub>1-x</sub>F<sub>x</sub>]FeAs ( $x = 0.05-0.12$ ) with  $T_c = 26$  K. *J. Am. Chem. Soc.* **130**, 3296–3297 (2008)
2. C. Wang, L. Li, S. Chi, Z. Zhu, Z. Ren, Y. Li, Y. Wang, X. Lin, Y. Luo, S. Jiang, X. Xu, G. Cao, Z. Xu, Thorium-doping-induced superconductivity up to 56 K in Gd<sub>1-x</sub>Th<sub>x</sub>FeAsO. *Europhys. Lett.* **83**, 67006 (2008)
3. G. Wu, Y.L. Xie, H. Chen, M. Zhong, R.H. Liu, B.C. Shi, Q.J. Li, X.F. Wang, T. Wu, Y.J. Yan, J.J. Ying, X.H. Chen, Superconductivity at 56 K in samarium-doped SrFeAsF. *J. Phys.: Condens. Matter* **21**, 142203 (2009)
4. T. Kikegawa, K. Sato, K. Ishikawa, Thermal conductivity and electrical resistivity of FeTe<sub>1-x</sub>S<sub>x</sub> sintered samples. *Phys. Procedia* **58**, 86–89 (2014)
5. Y. Mizuguchi, F. Tomioka, S. Tsuda, T. Yamaguchi, Y. Takano, FeTe as a candidate material for new iron-based superconductor. *Physica C* **469**, 1027–1029 (2009)
6. Y. Han, W.Y. Li, L.X. Cao, X.Y. Wang, B. Xu, B.R. Zhao, Y.Q. Guo, J.L. Yang, Superconductivity in iron telluride thin films under tensile stress. *Phys. Rev. Lett.* **104**, 017003 (2010)
7. A. Kjekshus, T. Rakke, Compounds with the marcasite type crystal structure. XI. High temperature studies of chalcogenides. *Acta Chem. Scand. A* **29**, 443 (1975)
8. D. Telesca, Y. Nie, J.I. Budnick, B.O. Wells, B. Sinkovic, Surface valence states and stoichiometry of non-superconducting and superconducting FeTe films. *Surf. Sci.* **606**, 1056–1061 (2012)
9. M. Bochmann, Metal chalcogenide materials: chalcogenolato complexes as “single-source” precursors. *Chem. Vap. Depos.* **2**, 85 (1996)
10. M.L. Steigerwald, T. Siegrist, S.M. Stuczynski, *Chem. Mater.* **114**, 3155 (1992)
11. X.J. Song, M. Bochmann, Synthesis of phosphinochalcogenoamidato complexes of divalent transition metals and their thermolysis to metal selenide and telluride phases. *J. Chem. Soc. Dalton Trans.* (1997). <https://doi.org/10.1039/A702460F>
12. K. Ben Messaoud, J. Ouerfelli, K. Boubaker, M. Amlouk, Structural properties of FeTe<sub>2</sub> thin films synthesized by tellurization of amorphous iron oxide thin films. *Mater. Sci. Semicond. Process.* **16**(6), 1912–1917 (2013)
13. K. BenMessaoud, A. Gantassi, H. Essaidi, J. Ouerfelli, A. Colantoni, K. Boubaker, M. Amlouk, Structural and optothermal properties of iron ditelluride layered structures in the framework of the lattice compatibility theory. *Adv. Mater. Sci. Eng.* (2014). <https://doi.org/10.1155/2014/534307>
14. A. Jebali, N. Khemiri, F. Aousgi, M. Ben Rabeh, M. Kanzari, Structural, morphological and optical properties of the sulfosalt material SnSb<sub>4</sub>S<sub>7</sub> thin films. *Mater. Sci. Semicond. Process.* **27**, 1057–1064 (2014)
15. B. Ouni, M. Haj Lakhdar, R. Boughalmi, T. Larbi, A. Boukhachem, A. Madani, K. Boubaker, M. Amlouk, Investigation of electrical and dielectric properties of antimony oxide (Sb<sub>2</sub>O<sub>4</sub>) semiconductor thin films for TCO and optoelectronic applications. *J. Non-Cryst. Solids* **367**, 1 (2013)
16. R. Boughalmi, A. Boukhachem, M. Amlouk, Optical and ac conductivity investigations on Sn doped Ag<sub>2</sub>S thin films under the structural transition framework. *Mater. Sci. Semicond. Process.* **30**, 218 (2015)
17. J. Guo, S. Liang, Y. shi, C. Hao, X. Wang, T.L. Ma, Electrocatalytic properties of iron chalcogenides as low-cost counter electrode materials for dye-sensitized solar cells. *RSC Adv.* (2015). <https://doi.org/10.1039/C5RA13147B>
18. P. Scherrer, Bestimmung der Größe und der inneren Struktur von Kolloidteilchen mittels Röntgenstrahlen. *Nach. Ges. Wiss. Göttingen* **1918**, 98 (1918)
19. H. Arifa, A. Boukhachem, B. Askri, K. Boubaker, A. Yumak, K. Raouadi, Structural, optical and conductivity investigations



- on  $\kappa$ -Al<sub>2</sub>O<sub>3</sub> ceramics for powder metallurgical production and sensitivity applications. *Ceram. Int.* **42**, 2147–2157 (2016)
20. O. Kamoun, A. Boukhachem, C. Mrabet, A. Yumak, P. Petkova, K. Boubaker, M. Amlouk, Effect of europium content on physical properties of In<sub>2</sub>O<sub>3</sub> thin films for sensitivity and optoelectronic applications. *Bull. Mater. Sci.* **39**, 777–788 (2016)
  21. N. Beji, M. Souli, M. Ajili, S. Azzaza, S. Alleg, N. Kamoun Turki, Effect of iron doping on structural, optical and electrical properties of sprayed In<sub>2</sub>O<sub>3</sub> thin films. *Superlattices Microstruct.* **81**, 114–128 (2015)
  22. A. Amlouk, K. Boubaker, M. Amlouk, A new procedure to prepare semiconducting ternary compounds from binary buffer materials and vacuum-deposited copper for photovoltaic applications. *Vacuum* **85**, 60–64 (2010)
  23. M. Souli, C. Nefzi, Z. Seboui, A. Mejri, R. Vidu, N. Kamoun-Turki, Improved structural properties, morphological and optical behaviors of sprayed Cu<sub>2</sub>ZnSnS<sub>4</sub> thin films induced by high gamma radiations for solar cells. *Mater. Sci. Semicond. Process.* **83**, 50–57 (2018)
  24. R. Mimouni, K. Boubaker, M. Amlouk, Investigation of structural and optical properties in cobalt-chromium co-doped ZnO thin films within the lattice compatibility theory scope. *J. Alloys Compd.* (2014). <https://doi.org/10.1016/j.jallcom.2014.11.016>
  25. N. Kamoun Allouchea, N. Jebbari, C. Guasch, N. Kamoun Turki, Influence of aluminum doping in CuInS<sub>2</sub> prepared by spray pyrolysis on different substrates. *J. Alloys Compd.* **501**, 85 (2010)
  26. V.K. Gudelli, V. Kanchana, S. Appalakondaiah, G. Vaitheeswaran, M.C. Valsakumar, Phase stability and thermoelectric properties of the mineral FeS<sub>2</sub>: an ab initio study. *J. Phys. Chem. C* **117**, 21120 (2013)
  27. A. Ghosh, R. Thangavel, Electronic structure and optical properties of iron based chalcogenide FeX<sub>2</sub> (X = S, Se, Te) for photovoltaic applications: a first principle study. *Indian J. Phys.* (2017). <https://doi.org/10.1007/s12648-017-1046-7>
  28. [extras.springer.com/2000/978-3-540-64966-3\\$4...s14d01.pdf](https://www.springer.com/2000/978-3-540-64966-3$4...s14d01.pdf)
  29. W. Si, Q. Jie, L. Wu et al., Superconductivity in epitaxial thin films of Fe<sub>1.08</sub>Te: O<sub>x</sub>. *Phys. Rev. B*, **81**(9), 092506 (2010)
  30. Y.F. Nie, D. Telesca, J.I. Budnick, B. Sinkovic, B.O. Wells, Superconductivity induced in iron telluride films by low-temperature oxygen incorporation. *Phys. Rev. B* **82**(2), 020508 (2010)
  31. W. Martienssen, Über die excitonenbanden der alkalihalogenidkristalle. *J. Phys. Chem. Solids* **2**, 257 (1957)
  32. O. Kamoun, A. Boukhachem, S. Alleg, B. Jeyadevan, M. Amlouk, Physical study of nano-structured MoO<sub>3</sub> films codoped with cobalt and nickel in which there is a ferro-diamagnetic transition. *J. Alloys Compd.* **741**, 847–854 (2018)
  33. P. Shikha, B.S. Randhawa, T. Si Kang, Greener synthetic route for superparamagnetic and luminescent α-Fe<sub>2</sub>O<sub>3</sub> nanoparticles in binary mixtures of ionic liquid and ethylene glycol. *RSC Adv.* **5**, 51158–51168 (2015)
  34. A.K. Jonscher, The ‘universal’ dielectric response. *Nature* **267**, 673 (1977)
  35. G.K. Prajapati, P.N. Gupta, Conduction mechanism in un-irradiated and c-irradiated PVA–H<sub>3</sub>PO<sub>4</sub> polymer electrolytes. *Nucl. Instrum. Methods Phys. Res. B* **267**, 3328–3332 (2009)
  36. C.R. Mariappan, G. Govindaraj, S.V. Rathan, G.V. Prakash, Vitri-fication of K<sub>3</sub>M<sub>2</sub>P<sub>3</sub>O<sub>12</sub> (M = B, Al, Bi) NASICON-type materials and electrical relaxation studies. *Mater. Sci. Eng. B* **123**, 63–68 (2005)
  37. N. Bitri, S. Dridi, F. Chaabouni, M. Abaab, Studies on the electrical properties of Cu<sub>2</sub>NiSnS<sub>4</sub> thin films prepared by a simple chemical method. *Mater. Lett.* (2017). <https://doi.org/10.1016/j.matlet.2017.11.006>
  38. A. Mami, R. Boughalmi, S. Lazzez, I. Mellouki, N. Yacoubi, M. Amlouk, Determination of thermal properties of some sulfide thin films using electropyroelectric method. *J. Therm. Anal. Calorim.* (2018). <https://doi.org/10.1007/s10973-018-7863-x>
  39. A. Mami et al., Deep thermal investigations on Ag<sub>2</sub>S thin film along with electro-pyroelectric and photothermal deflection technique. *IEEE Sens. J.* **16**(23), 8374–8380 (2016)
  40. O. Dachraoui, J.M. Merino, A. Mami, M. León, R. Caballero, H. Maghraoui Meherzi, Annealing study and thermal investigation on bismuth sulfide thinfilms prepared by chemical bath deposition in basic medium. *Appl. Phys. A* **124**, 166 (2018)
  41. K. Wang, R. Hu, C. Petrovic, Significant suppression of thermal conductivity in FeSb<sub>2</sub> by Te doping. arXiv preprint arXiv:1102.0553, 2011 - arxiv.org
  42. A. Datta, G.S. Nolas, Synthesis and characterization of nanocrystalline FeSb<sub>2</sub> for thermoelectric applications. *Eur. J. Inorg. Chem.* **2012**, 55–58 (2012)
  43. K. Mageshwari et al., Template-free synthesis of MgO nanoparticles for effective photocatalytic applications. *Powder Technol.* **249**, 456–462 (2013)
  44. Y. Zhang, J. Mu, One-pot synthesis, photoluminescence, and photocatalysis of Ag/ZnO composites. *J. Colloid Interface Sci.* **309**, 478–484 (2007)
  45. N. Sobana, M. Swaminathan, Combination effect of ZnO and activated carbon for solar assisted photocatalytic degradation of direct blue. *Sol. Energy Mater. Sol. Cells* **91**, 727–734 (2007)
  46. X. Li, Y. Cheng, S. Kang, J. Mu, Preparation and enhanced visible light-driven catalytic activity of ZnO microrods sensitized by porphyrin heteroaggregate. *Appl. Surf. Sci.* **256**, 6705–6709 (2010)
  47. C.V. Reddy, B. Babu, J. Shim, Synthesis, optical properties and efficient photocatalytic activity of CdO/ZnO hybrid nanocomposite. *J. Phys. Chem. Solids* (2017). <https://doi.org/10.1016/j.jpcs.2017.09.003>

**Publisher’s Note** Springer Nature remains neutral with regard to jurisdictional claims in published maps and institutional affiliations.